FINITE ELEMENT BUCKLING AND POSTBUCKLING ANALYSIS OF PULTRUDED FRP I-SECTION COLUMNS

F. Laudiero[1], F. Minghini[1*], N. Tullini[1]

[1]*Engineering Department, University of Ferrara, via Saragat 1, 44122 Ferrara, Italy*
**fabio.minghini@unife.it*

Keywords: PFRP; I-section; buckling-mode interaction; postbuckling analysis.

Abstract
The present work puts in evidence some interesting features of Pultruded Fibre-Reinforced Plastic (PFRP) I-section columns. A finite-element model of a commercial I-section shape with dimensions 305×152×12.7 mm was implemented using four-node orthotropic plate elements. Ten column lengths were investigated, covering the range from stocky up to very slender columns. A nonlinear analysis of buckling and postbuckling was carried out using the displacement control method. It was observed that, in the case of stocky columns, the ultimate conditions are governed by the web failure, whereas, in the case of slender columns, the high longitudinal compressive stresses attained lead to the flange failure. With respect to a wide-flange shape by the same pultruder and with equal cross-section area, the I-section column shows a higher ultimate resistance in a broad range of column lengths.

1 Introduction

In PFRP short columns with wide-flange (WF) section subjected to axial compression, the instability is triggered by the flange buckling (see [1]) and the ultimate conditions are governed by the strength of the web-flange junctions, [2]. In slender WF columns, the interaction between global and local buckling modes may occur (see [3]) and the ultimate resistance is strongly influenced by the amplitude of the initial imperfection, [4]. With regard to PFRP narrow-flange (I-section) profiles, less information is available, since WF columns are generally preferred for construction. However, I-section columns are characterized by some interesting features, which the present work tries to explain. A finite-element model of a commercial I-section shape with dimensions 305×152×12.7 mm was implemented using four-node orthotropic plate elements. Ten column lengths were investigated, covering the range from stocky up to very slender columns. A geometric nonlinear analysis was carried out by imposing an incremental column shortening to the end section centroids. The failure mechanisms of the column are discussed in the paper, and a comparison with a WF shape of the same pultruder and with similar cross-section area is presented.

2 Analytical buckling loads

The equations presented in the following apply to WF- or I-section columns with length L, cross-section height H, flange width b_f and, finally, web and flange thicknesses t_w and t_f, respectively (Figure 1a).

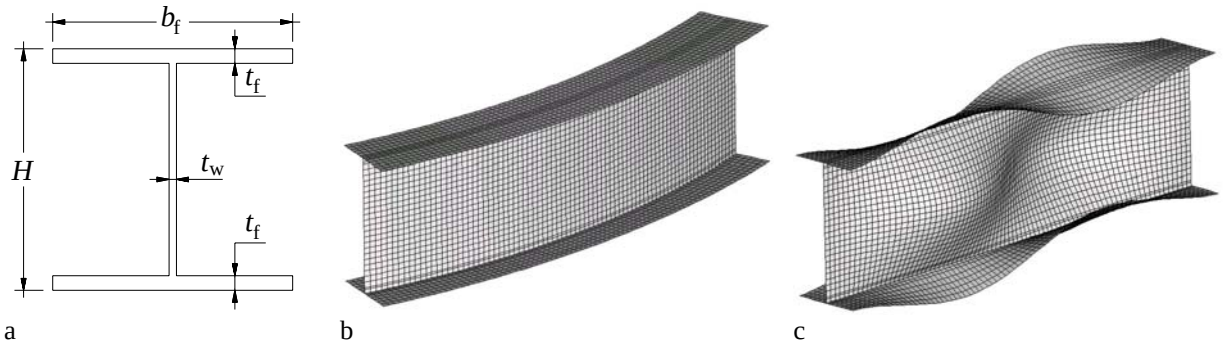

Figure 1. Column cross-section (a) and shapes of S- (b) and F-imperfection (c).

Column section dimensions mm	E_{eff} GPa	A $m^2\times10^{-3}$	J_{min} $m^4\times10^{-5}$	D_{11} $Nm\times10^3$	D_{22} $Nm\times10^3$	D_{12} $Nm\times10^3$	D_{66} $Nm\times10^3$
305×152×12.7 (I)	17.2	7.426	0.754	3.052	1.064	0.351	0.495
254×254×9.5 (WF)	17.2	7.084	2.600	1.290	0.450	0.148	0.209

Table 1. Full-section properties and laminate bending stiffnesses for the two column sections, [6].

Column section		Slenderness λ_P									
		0.4	0.6	0.8	0.9	1.0	1.1	1.2	1.3	1.4	1.5
I	*L*	694.4	1041.6	1388.8	1562.4	1736.0	1909.6	2083.2	2256.8	2430.4	2604.0
	n	2916	4428	5940	6588	6528	7200	7872	8544	9216	9792
WF	*L*	1919.4	2879.1	3838.8	4318.6	4798.5	5278.3	5758.2	6238.0	6717.9	7197.7
	n	10032	14916	19932	22440	22680	24960	27240	29520	31680	33960

Table 2. Column lengths *L* (in mm) and corresponding numbers of finite elements (n).

Strength property		Symbol	Nominal strength (MPa)
Web and flanges	Longitudinal tensile strength	f_{Lt}	207.0
	Longitudinal compressive strength	f_{Lc}	207.0
	Transverse tensile strength	f_{Tt}	48.3
	Transverse compressive strength	f_{Tc}	103.0
	In-plane shear strength	f_V	31.0
Web-flange junctions	Longitudinal compressive strength	$f_{Lc,j}$	207.0
	Bending strength	$f_{Tf,j}$	68.9
	Shear strength	$f_{V,j}$	31.0

Table 3. Strength values for the two columns analyzed, [6].

2.1 Global buckling

For a slender PFRP column in compression, the global buckling load may be estimated (see [5], [6]) using the Euler formula:

$$P_{Eul} = \pi^2 E_{eff} J_{min} / (kL)^2 \tag{1}$$

where coefficient k takes account of the end restraints (k = 1 for a simply supported column) and E_{eff} and J_{min} (see Table 1 for the shapes analyzed) are the effective modulus of elasticity (see [7]) and the second moment of area with respect to the minor-axis, respectively.

2.2 Local buckling

With regard to the local buckling problem for stocky pultruded columns, several analytical solutions and parametric analyses are available, [8]–[10]. Hereafter, the explicit expressions

for the critical normal stresses given in [11] under the long-plate hypothesis are used. In particular, if web and flanges are considered separately from each other and regarded as orthotropic plates in uniaxial compression elastically restrained along their common edges (i.e. the web-flange junctions), the buckling load may be given the following form:

$$P_{\text{loc}} = A \cdot \min\left\{ f_{\text{cr,f}} ; f_{\text{cr,w}} \right\} \tag{2}$$

where A is the cross-section area (Table 1) and $f_{\text{cr,f}}$ and $f_{\text{cr,w}}$ indicate the critical normal stresses of flanges (index "f") and web (index "w"), respectively. The critical normal stress of the flanges can be written as (see [11]):

$$f_{\text{cr,f}} = \sqrt{D_{11,\text{f}} D_{22,\text{f}}} \left\{ K \left[15.1\eta\sqrt{1-\upsilon} + 6(1-\eta)(1-\upsilon) \right] + 7(1-K) \Big/ \sqrt{1+4.12\zeta} \right\} \Big/ \left[t_{\text{f}} \left(b_{\text{f}} / 2 \right)^2 \right] \tag{3}$$

if $K \leq 1$ and

$$f_{\text{cr,f}} = \sqrt{D_{11,\text{f}} D_{22,\text{f}}} \left[15.1\eta\sqrt{1-\upsilon} + 6(K-\eta)(1-\upsilon) \right] \Big/ \left[t_{\text{f}} \left(b_{\text{f}} / 2 \right)^2 \right] \tag{4}$$

if $K > 1$. In Eqs. (3) and (4), $\upsilon = D_{12,\text{f}} / \left(D_{12,\text{f}} + 2D_{66,\text{f}} \right)$, $K = \left(D_{12,\text{f}} + 2D_{66,\text{f}} \right) \Big/ \sqrt{D_{11,\text{f}} D_{22,\text{f}}}$, $\eta = 1 \Big/ \sqrt{1 + (7.22 - 3.55\upsilon)\zeta}$ and $\zeta = 2D_{22,\text{f}} / \left(\tilde{k}_{\text{f}} b_{\text{f}} \right)$, where

$$\tilde{k}_{\text{f}} = D_{22,\text{w}} / \left[r \left(H - t_{\text{f}} \right) \right] \tag{5}$$

represents the rotational spring stiffness reproducing the restraining effect exerted by the web on each half flange. The critical normal stress of the web can be written as (see [11]):

$$f_{\text{cr,w}} = \pi^2 \left[2\sqrt{1+4.139\xi} \sqrt{D_{11,\text{w}} D_{22,\text{w}}} + \left(2 + 0.62\xi^2 \right) \left(D_{12,\text{w}} + 2D_{66,\text{w}} \right) \right] \Big/ \left[t_{\text{w}} \left(H - t_{\text{f}} \right)^2 \right] \tag{6}$$

where $\xi = 1 \Big/ \left(1 + 0.61\zeta'^{1.2} \right)$ and $\zeta' = D_{22,\text{w}} b_{\text{w}} \Big/ \tilde{k}_{\text{w}}$, being

$$\tilde{k}_{\text{w}} = 4D_{66,\text{f}} b_{\text{f}} / r \tag{7}$$

the torsional stiffness of the flanges reproducing the restraining effect exerted by the flanges on the web. Coefficients $D_{11,\text{i}}$, $D_{22,\text{i}}$, $D_{12,\text{i}}$ and $D_{66,\text{i}}$ (i = f, w) appearing in the previous equations are the bending stiffnesses of the wall segments of the cross-section, [5]. The bending stiffnesses of the two column section analyzed are reported in Table 1, where the index has been dropped, since identical elastic properties for web and flanges are provided by the pultruder. Coefficient r in Eqs. (5) and (7) is an amplification factor depending on the axial compression and is given by:

$$r = \left(1 - f_{\text{cr,f}}^{\text{SS}} a_{11,\text{f}} \Big/ f_{\text{cr,w}}^{\text{SS}} a_{11,\text{w}} \right)^{-1} \tag{8}$$

if $f_{\text{cr,f}}^{\text{SS}} a_{11,\text{f}} < f_{\text{cr,w}}^{\text{SS}} a_{11,\text{w}}$ or by:

$$r = \left(1 - f_{\mathrm{cr,w}}^{\mathrm{SS}} a_{11,\mathrm{w}} \,/\, f_{\mathrm{cr,f}}^{\mathrm{SS}} a_{11,\mathrm{f}}\right)^{-1} \tag{9}$$

if $f_{\mathrm{cr,f}}^{\mathrm{SS}} a_{11,\mathrm{f}} > f_{\mathrm{cr,w}}^{\mathrm{SS}} a_{11,\mathrm{w}}$, where

$$f_{\mathrm{cr,f}}^{\mathrm{SS}} = 12 D_{66,\mathrm{f}} \,/\left[t_{\mathrm{f}} \left(b_{\mathrm{f}}/2\right)^2\right] \tag{10}$$

$$f_{\mathrm{cr,w}}^{\mathrm{SS}} = \pi^2 \left[2\sqrt{D_{11,\mathrm{w}} D_{22,\mathrm{w}}} + 2\left(D_{12,\mathrm{w}} + 2D_{66,\mathrm{w}}\right)\right] \Big/ \left[t_{\mathrm{w}} \left(H - t_{\mathrm{f}}\right)^2\right] \tag{11}$$

represent the critical stresses of half-flanges and web, respectively, considered as long plates simply supported ("SS") along the web-flange junctions. In Eqs. (8) and (9), $a_{11,\mathrm{i}}$ (i = f, w) is the tensile compliance of flange or web panels ($a_{11,\mathrm{f}} = a_{11,\mathrm{w}} = a_{11}$ for the two column sections analyzed). For WF-section columns, the condition $f_{\mathrm{cr,f}}^{\mathrm{SS}} a_{11,\mathrm{f}} < f_{\mathrm{cr,w}}^{\mathrm{SS}} a_{11,\mathrm{w}}$ generally occurs and the local buckling load P_{loc} turns out to be given by $Af_{\mathrm{cr,f}}$, with $f_{\mathrm{cr,f}}$ provided by Eq. (3) or by Eq. (4). In contrast, for I-section columns, the condition $f_{\mathrm{cr,f}}^{\mathrm{SS}} a_{11,\mathrm{f}} > f_{\mathrm{cr,w}}^{\mathrm{SS}} a_{11,\mathrm{w}}$ generally occurs, yielding $P_{\mathrm{loc}} = Af_{\mathrm{cr,w}}$, with $f_{\mathrm{cr,w}}$ provided by Eq. (6). In the following, the use of Eq. (6), with the restraint stiffness given by Eq. (7), will be referred to as the elastically restrained web (ERW) approximation, whereas the more conservative assumption $P_{\mathrm{loc}} = P_{\mathrm{loc,SSW}} = Af_{\mathrm{cr,w}}^{\mathrm{SS}}$, with $f_{\mathrm{cr,w}}^{\mathrm{SS}}$ given by Eq. (11), will be referred to as the simply supported web (SSW) approximation. A universal slenderness ratio is usually defined as (see [12]):

$$\lambda_P = \sqrt{P_{\mathrm{loc}} / P_{\mathrm{Eul}}} \tag{12}$$

depending on the two individual buckling loads given by Eqs. (1) and (2).

3 Finite element modelling

Four-node orthotropic plate elements (see [13]) were used and preliminary convergence rate tests were carried out to optimize the mesh size. The meshes were located on the middle surface of the flanges and the web. The slenderness ratios λ_P and the corresponding lengths L of the columns analyzed are reported in Table 2. At the same time, for each λ_P, the table provides the number n of finite elements used for the analysis. The end sections were assumed to remain plane, since warping deformations do not play a significant role in the experimental tests [2]. Hence, the simple support condition was reproduced using master-slave elements to force the column end cross-sections to rotate rigidly about their principal inertia axes while preventing any in-plane displacement, [3].

3.1 Initial imperfections

Two different imperfection shapes were taken into account with reference to the following dimensional tolerances: straightness ("S") and flatness ("F"). In particular, the S-imperfection was assumed in the shape of the first global buckling mode (Figure 1b) and reproduced through end moments acting about the minor-axis, [3]. The F-imperfection was assumed to be proportional to the first local buckling mode (Figure 1c) and reproduced by five force distributions varying with sinusoidal law along the flange edges and the centreline of the web (see [3]). Two sets of amplitudes were considered for the imperfection shapes. In the first set, the limiting tolerances indicated by the American standard [14], i.e. $L/240$ for the S-imperfection and $8.0 \cdot 10^{-3} H$ for the F-imperfection (see also [7]), were adopted. In the second

set, reduced amplitudes were used in accordance with the general high standard of manufacture, i.e. $L/4500$ for the S-imperfection (see [4]) and $2.0 \cdot 10^{-5} H$ for the F-imperfection, [2].

3.2 Failure criteria

Stress checks were performed in the post-processing phase following [2], where the Tsai–Wu criterion (see [15]) was used to determine the onset of failure in the web and the flanges of the columns, whereas a quadratic failure criterion was proposed for the web-flange junctions. However, the web-flange junction data for the pultruded shapes analyzed in the this work are not available at the present and so conservative estimates of the strengths required were adopted (see [3], [16]). In particular, transverse bending and interlaminar shear strengths of the web (see [6]) were used in place of bending and shear strengths of the web-flange junction, respectively. The strength values used in the failure criteria are reported in Table 3.

4 Numerical results

The FE computed P-δ curves of the I-section column, being δ the centroidal column displacement in the minor-axis plane, are reported in Figure 2a and Figure 2b for $\lambda_P = 0.4$ and $\lambda_P = 1.3$, respectively. For the stocky column (Figure 2a), the web buckling prevails and $P_{\text{loc,ERW}}$ and $P_{\text{loc,SSW}}$ indicate the local buckling loads corresponding to the ERW and the SSW approximations (see Section 2.2), respectively. The curves labeled F and S in Figure 2a indicate the numerical results for the column with F- and S-imperfection, respectively, and amplitude equal to the corresponding limiting tolerance (see Section 3.1). Analogously, "F red." and "S red." refer to the reduced set of imperfection amplitudes. Due to the stable postbuckling behaviour exhibited by the orthotropic plates in uniaxial compression (see [17]), the resisting force P significantly exceeds the local buckling load, especially for the reduced imperfection amplitudes. As a matter of fact, in this case, the ultimate conditions correspond to failure at the mid-depth of the web and the ultimate column load obtained is $P_u = 641.3$ kN (curve S red.) or $P_u = 652.2$ kN (curve F red.). The web failure was also observed for the F-imperfection with the limiting amplitude (curve F), but in correspondence of $P_u = 485.0$ kN. In contrast, for the S-imperfection with the limiting amplitude (curve S), the flange failure was observed due to the significant minor-axis sweep, and the column resistance turned out to be $P_u = 517.1$ kN.

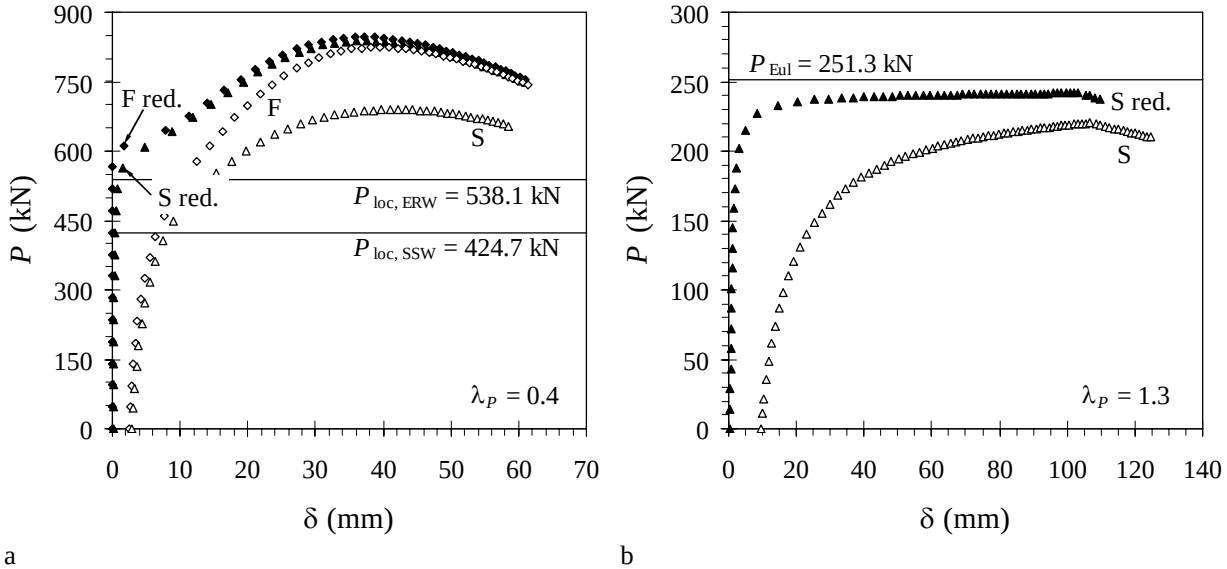

Figure 2. FE computed P-δ curves of the I-section column for $\lambda_P = 0.4$ (a) and $\lambda_P = 1.3$ (b).

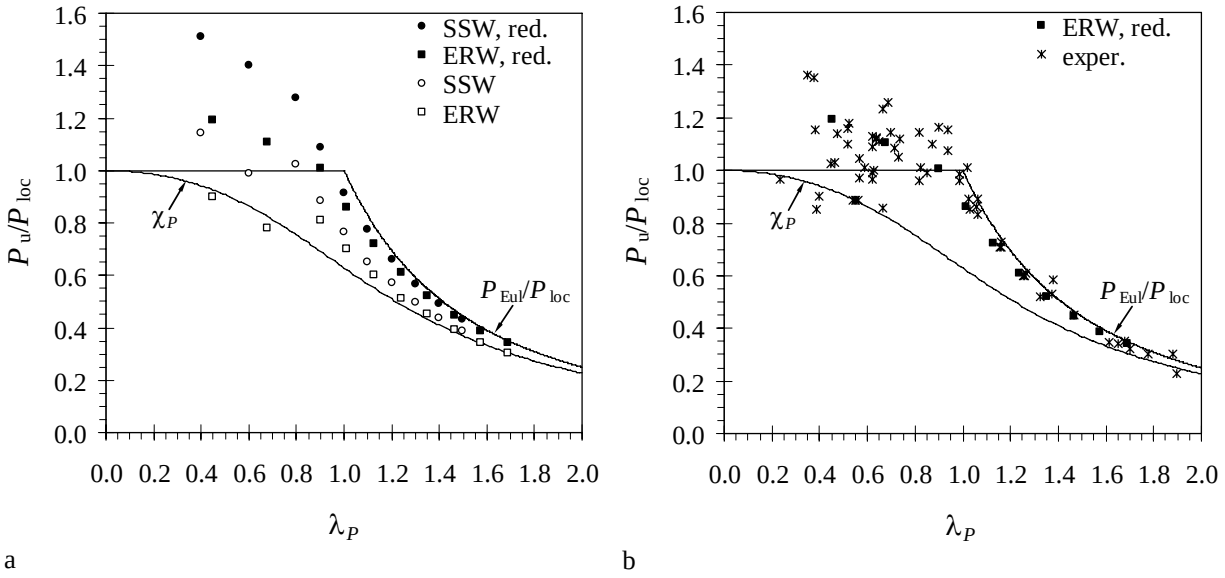

Figure 3. FE predicted ultimate column loads compared with local and global buckling and buckling interaction design curves (a). Comparison between numerical results and experimental failure loads from [20] (b).

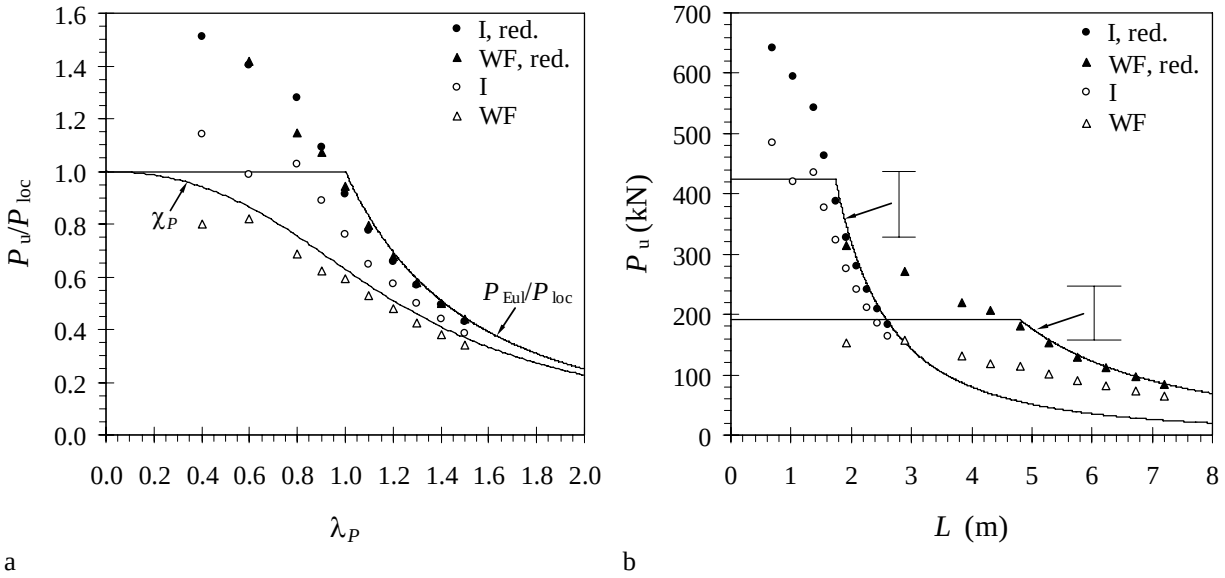

Figure 4. FE predicted ultimate column loads of the I- and the WF-section profiles reported versus the slenderness ratio λ_P in nondimensional form (a) and versus del column length L (b).

For the slender column (Figure 2b), the global instability prevails and the numerical solutions are compared with P_{Eul} from Eq. (1). In particular, for the reduced imperfection amplitude (curve S red.), a bifurcation load P_b = 241.8 kN, followed by a descending branch, is attained in correspondence of δ = 103.3 mm. It corresponds to the onset of interaction between the global and the flange buckling. Yet, due to the flange failure of the column undergoing a large minor-axis sweep, the ultimate load is P_u = 240.9 kN < P_b and corresponds to δ = 75.8 mm. The solution for the S-imperfection with the limiting amplitude (curve S) is qualitatively similar, but P_b = 220.3 kN and P_u = 211.5 kN for δ = 106.5 mm and 78.0 mm, respectively. The failure mechanism described, observed also for λ_P = 1, 1.1, 1.2, 1.4 and 1.5, was documented in [18].

4.1 Ultimate column loads of the I-section profile

The ultimate column loads P_u obtained by the FE analysis are reported in nondimensional form in Figure 3a versus the slenderness ratio λ_P. In particular, two different nondimensionalizations, corresponding to the ERW and the SSW approximations (see Section 2.2), are used in the figure. Moreover, the results obtained for both the limiting and the reduced values of the imperfection amplitudes are reported. Finally, for the columns with λ_P = 0.4, 0.6, 0.8 and 0.9, the reported value of P_u is the minimum between that for the F- and that for the S-imperfection. In the same figure, the full lines represent the two independent buckling loads and the buckling interaction design curve provided in [12], i.e.:

$$\chi_P = \left(\Phi_P - \sqrt{\Phi_P^2 - c_P\lambda_P^2}\right) \Big/ \left(c_P\lambda_P^2\right) \tag{13}$$

where $\Phi_P = \left(1+\lambda_P^2\right)/2$ and c_P = 0.65 (see [19]). It can be noted that, with respect to the limiting tolerances, the reduced set of imperfection amplitudes yields a significant improvement in the column resistance for all λ_P considered. In Figure 3b, the nondimensional ($P_{loc} = P_{loc,ERW}$) ultimate column loads for the reduced set of imperfection amplitudes seem to fit well, on average, the experimental failure loads of WF columns (adapted from [20]).

4.2 Comparison with a WF-column with equal cross-section area

A WF-section column by the same pultruder was then selected for comparison purposes (Table 1). In particular, with respect to the I-section column analyzed, area and bending rigidity in the minor-axis plane of the WF-section are about 4.5% less and 245% larger, respectively. The local buckling mode of the WF column is dominated by the flange buckling (see Section 2.2) and P_{loc} = 191.9 kN. When the ultimate loads of the I-section column are reported in nondimensional form for $P_{loc} = P_{loc,SSW}$ (Figure 4a), a substantial equivalence between the two pultruded shapes is observed if imperfections with reduced amplitudes are considered, whereas the limiting imperfection amplitudes dramatically affect the WF column. As a matter of fact, when the ultimate column loads P_u are reported versus the column length L (Figure 4b), the I-section profile shows a better performance in a wide range of column lengths, i.e. $L \leq 2$ up to about 3 m, depending on the imperfection amplitudes.

5 Conclusions

The failure mechanism of the I-section shape analyzed is triggered by the web buckling for L up to about 1.5 m. Hence, with respect to a WF column with nominally identical axial load capacity (i.e., with equal cross-section area and longitudinal compressive strength), the I-section column performs better for L less or equal to 2 up to about 3 m, depending on the imperfection amplitude.

6 Acknowledgements

The present investigation was developed in the framework of the National (Italian) Research Program n. 20089RJKYN coordinated by Prof. Paolo Bisegna from University of Rome ‘‘Tor Vergata’’ and of the Research Program FAR 2011 of the University of Ferrara. Moreover, the analyses were developed within the activities of the (Italian) University Network of Seismic Engineering Laboratories–ReLUIS – Progetto Esecutivo 2010-2013 – Research Line 3, coordinated by Profs. Luigi Ascione and Giorgio Serino.

References

[1] Tomblin J., Barbero E.J. Local buckling experiments on FRP columns. *Thin-Walled Structures*, **18**, pp. 97-116 (1994).

[2] Turvey G.J., Zhang Y. A computational and experimental analysis of the buckling, postbuckling and initial failure of pultruded GRP columns. *Computer & Structures*, **84**, pp. 1527-1537 (2006).
[3] Laudiero F., Minghini F., Ponara N., Tullini N. *Buckling resistance of pultruded FRP profiles under pure compression or uniform bending—Numerical simulation* in "Proceedings of the 6th *International Conference on FRP Composites in Civil Engineering (CICE 2012)*", Rome, Italy (2012).
[4] Mottram J.T., Brown N.D., Anderson D. Physical testing for concentrically loaded columns of pultruded glass fibre reinforced plastic profile. *Proceedings of the Institution of Civil Engineers, Structures and Buildings Journal*, **158**, pp. 205-219 (2003).
[5] Kollár L.P., Springer G.S. *Mechanics of composite structures*. Cambridge University Press, Cambridge (2003).
[6] Strongwell. *Design manual—EXTREN® and other proprietary pultruded products*. Rev. 0910, © 2010 Strongwell Corporation, Bristol (2010).
[7] BS EN 13706-2:2002. *Reinforced plastics composites—Specifications for pultruded profiles—Part 2: Method of test and general requirements* (2002).
[8] Bank L.C., Yin J. Buckling of orthotropic plates with free and rotationally restrained unloaded edges. *Thin-Walled Structures*, **24**, pp. 83-96 (1996).
[9] Qiao P., Davalos J.F., Wang J. Local buckling of composite FRP shapes by discrete plate analysis. *Journal of Structural Engineering, ASCE*, **127**, pp. 245-255 (2001).
[10] Shan L. *Explicit buckling analysis of fiber-reinforced plastic (FRP) composite structures*. PhD thesis, Washington State University, Department of Civil and Environmental Engineering (2007).
[11] Kollár L.P. Local buckling of fiber reinforced plastic composite structural members with open and closed cross sections. *Journal of Structural Engineering, ASCE*, **129**, pp. 1503-1513 (2003).
[12] Barbero E.J., Tomblin J. A phenomenological design equation for FRP columns with interaction between local and global buckling. *Thin-Walled Structures*, **18**, pp. 117-131 (1994).
[13] STRAUS7®. *Theoretical manual—theoretical background to the Straus7 finite element analysis system*. First ed., G+D Computing Pty Ltd, Sidney (2005).
[14] ASTM D 3917-08. *Standard specification for dimensional tolerance of thermosetting glass-reinforced plastic pultruded shapes* (2008).
[15] Tsai S.W., Wu E.M. General theory of strength for anisotropic materials. *Journal of Composite Materials*, **5**, pp. 58-80 (1971).
[16] Turvey G.J., Zhang Y. Characterisation of the rotational stiffness and strength of web-flange junctions of pultruded GRP WF-sections via web bending tests. *Composites Part A: Applied Science and Manufacturing*, **37**, pp. 152-164 (2006).
[17] Cui E.J., Dowell E.J. Postbuckling behaviour of rectangular orthotropic plates with two free side edges. *International Journal of Mechanical Sciences*, **25**, pp. 429-446 (1983).
[18] Barbero E.J., Turk M. Experimental investigation of beam-column behavior of pultruded structural shapes. *Journal of Reinforced Plastics and Composites*, **19**, pp. 249-265 (2000).
[19] CNR DT 205/2007. *Guide for the design and construction of structures made of thin FRP pultruded elements*. National Research Council of Italy (CNR), Rome (2008). Available online at www.cnr.it.
[20] Vanevenhoven L.M., Shield C.K, Bank L.C. LRFD factors for pultruded wide-flange columns. *Journal of Structural Engineering, ASCE*, **136**, pp. 554-564 (2010).